A versatile DNA origami based plasmonic nanoantenna for label-free single-molecule SERS

Kosti Tapio
University of Potsdam
Amr Mostafa
University of Potsdam
Yuya Kanehira
University of Potsdam
Antonio Suma
Temple University https://orcid.org/0000-0002-5049-9255
Anushree Dutta
University of Potsdam
Ilko Bald (bald@uni-potsdam.de)
University of Potsdam

Article

Keywords: DNA Origami Nanofork Antenna, surface-enhanced Raman scattering, single molecules, nanomachines

Posted Date: December 28th, 2020

DOI: https://doi.org/10.21203/rs.3.rs-47458/v2

A versatile DNA origami based plasmonic nanoantenna for label-free single-molecule SERS

Kosti Tapio[1], Amr Mostafa[1], Yuya Kanehira[1], Antonio Suma[2,3], Anushree Dutta[1], Ilko Bald[1*]

[1]*Institute of Chemistry, University of Potsdam, Potsdam, Germany*

[2]*Institute for Computational Molecular Science, Temple University, Philadelphia, Pennsylvania, USA*

[3]*Dipartimento di Fisica, Università di Bari, and Sezione INFN di Bari, Bari, Italy*

*corresponding author: ilko.bald@uni-potsdam.de

Abstract

DNA origami technology allows for the precise nanoscale assembly of chemical entities that give rise to new functional materials. We have created a versatile DNA Origami Nanofork Antenna (DONA) by assembling Au or Ag nanoparticle dimers with different gap sizes down to 1.17 nm, enabling signal enhancements in surface-enhanced Raman scattering (SERS) of up to 10^{11}. This allows for single-molecule SERS measurements, which can even be performed with larger gap sizes to accommodate differently sized molecules, and at various excitation wavelengths. A general scheme is presented to place single analyte molecules into the SERS hot spots using the DNA origami structure exploiting covalent and non-covalent coupling schemes. By using Au and Ag dimers, single-molecule SERS measurements of three dyes and cytochrome c and horseradish peroxidase proteins are demonstrated even under non-resonant excitation conditions, thus providing long photostability during time-series measurement, and enabling unprecedented optical monitoring of single molecules.

The ultimate detection limit in analytical chemistry is the single molecule (SM), ideally without the necessity to label the target molecule. Furthermore, the ability to extract specific information about single molecular events allows for the screening of molecular property distributions, which are otherwise hidden within an ensemble averaged measurement.(*1*) Up to now, several techniques have been reported that are capable of detecting molecules down to the SM regime , such as fluorescence spectroscopy,(*2*) scanning probe microscopy,(*3*) and surface enhanced Raman scattering (SERS).(*4*) Among them, SERS is a particularly promising technique because in addition to the simple detection of a target molecule, it can also provide detailed chemical and structural information through the Raman vibrational fingerprint of the molecule. However, SERS relies on the strong Raman signal enhancement upon excitation of localised surface plasmon resonances (LSPR), mainly in gold (Au) or silver (Ag) nanostructures.(*5, 6*) The Raman signal enhancement is the strongest in small, nanometer-sized volumes in-between coupled Au or Ag nanostructures, which are referred to as SERS hot spots. Therefore, the detection of single molecules in these hot spots requires a precise control over the arrangement of nanoparticles as well as the placement of target molecules into these hot spots, which imposes severe challenges for nanofabrication. This is why most of the single-molecule SERS measurements reported so far rely on the random adsorption of analyte molecules in the hot spots.(*4, 7, 8*) In a complementary approach the analyte molecules are precisely positioned into the hot spots *via* covalent or non-covalent interactions using DNA.(*9*) DNA origami is a powerful nanoengineering tool,(*10*) which is based on the programmed self-assembly into various 2D and 3D shapes.(*11, 12*) DNA origami nanostructures are formed from a long single-stranded scaffold strand and a suitable set of short artificial staple strands(*10*) and several computation tools have been developed to automate the design process of DNA origami.(*13–17*) Due to the rich chemical functionalization schemes of DNA, molecules can be positioned along the DNA origami surface with nanometer precision.(*18*) Furthermore, various kinds of nanoparticles can be arranged on the nanoscale to create sophisticated plasmonic nanostructures and to perform SERS(*19–28*) and surface enhanced fluorescence (SEF)(*29, 30*) measurements. Past examples of such structures include different platforms to form dimers of spherical particles(*19, 26, 29, 31–33*), dimers of Au nanostars(*27*), bowtie antennas(*28*), bimetallic

nanostructures(*20, 32*), DNA origami nanocavities,(*34, 35*) and plasmonic nanostructures consisting of three or more spherical particles.(*21, 22, 24, 36*) While DNA origami based nanoantennas with larger interparticle gaps in the range of 10-30 nm are required for SEF, SERS requires small gaps below about 5 nm to provide strong signal enhancement. Consequently, DNA origami based single-molecule SERS measurements have mainly focussed on small molecules such as organic dyes that can be placed in small interparticle gaps either by random adsorption or by DNA-conjugation. Here, we introduce a new and versatile three-dimensional (3D) plasmonic DNA Origami Nanofork Antenna (DONA) structure representing Au and Ag dimers suitable for SM SERS measurements of not just small molecules or DNA, but also more complex biomolecules such as cytochrome c (cyt c) and horseradish peroxidase (HRP). Through oxDNA simulation and atomic force microscopy (AFM), we can demonstrate that the structure exhibits better overall rigidity compared to the previous SERS substrates and the ability to place biomolecules precisely into the dimeric hot spot. The addressable binding sites in the as-designed DONA structures allow for precise placement of basically arbitrary molecules of different dimension in the gap between two Au or Ag nanoparticles, where the electric field enhancement is strong enough to detect single molecules by SERS. Here, the increase in the gap size to accommodate larger molecules come in the expense of lowered field enhancement in the hot spot but with the increase of the overall hot spot volume. By varying the gap size, we can show that DONAs with larger gap sizes can still produce single-molecule signals, although the DONAs with smaller gap sizes are flexible enough to accommodate proteins to produce a high yield of single molecule SERS spectra. Our findings suggest that the proteins, even though having the dimensions larger than the gap size, can at least partially occupy the hot spot and thus exhibit characteristic Raman spectra.

Results

To create complex arrangements of Au and Ag nanoparticles on DNA origami nanostructures the particles are coated with thiolated single-stranded DNA that is hybridized to complementary DNA extensions protruding from the DNA origami.(*21, 37, 38*) A frequently used nanoparticle configuration

for SERS is the nanoparticle dimer. Importantly, even a small offset from the hot spot can lead to a drastic drop in the field enhancement, which calls for precise positioning of molecules in-between the nanoparticles, which however, has been challenging. To overcome this, we have designed a DNA origami nanofork structure forming the basis of the plasmonic DONA structures. It consists of a rectangular base with two arms, as is illustrated in Fig. 1A and Fig. S1 (Supplementary Information, SI). Two nanoparticles can be bound to the arms such that each particle is connected to both arms. The two arms are connected by a bridge consisting of two DNA double helices. The main purpose of the bridge is to serve as an anchor point for target analyte molecules, which can be precisely placed into the plasmonic gap of the two nanoparticles, at the location where the SERS signal enhancement is the strongest.

The outer dimensions of the DNA origami nanofork are estimated to be 48 nm x 71 nm, based on an inter-helical distance of 2.536 nm for a honeycomb lattice.(*39*) The distance between the two arms is designed to be about 31 nm. Each arm is equipped with four ssDNA capture strands (capture sequences **a** = 5'-A_{24} and **b** = 3'-$(AAC)_8$ in Fig. 1 and Fig. S1, to bind two differently coated nanoparticles), extending to different sides and designed to bind complementary sequences on Au or Ag nanoparticles. The bridge includes four staple strands, each crossing over once between the two helices to increase the stability and rigidity of the bridge. In addition, the free 3' and 5' ends of these staple strands allow for modifications to be added to the bridge. Further, to increase the precision of the nanoparticle placement, two of the bridge staple strands are equipped with capture strands on each end. Hence, each nanoparticle will be bound by a total of six capture strands.

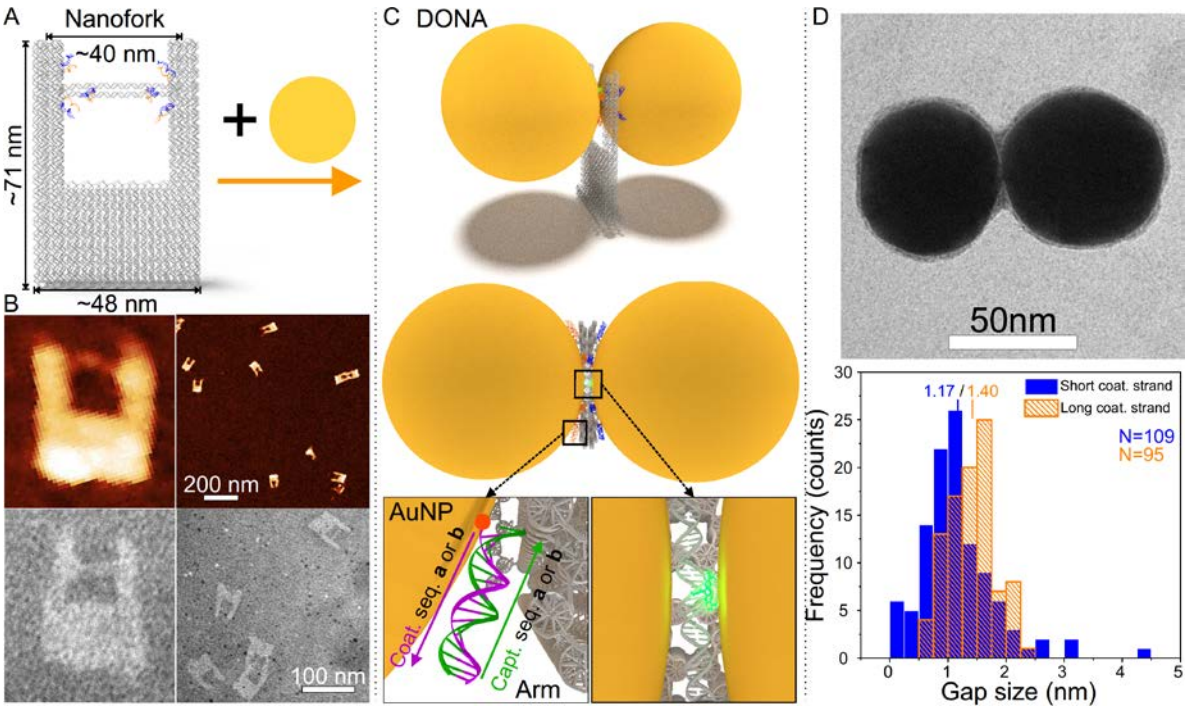

Fig. 1. Scheme and characterization of the DONA structures. (A) Schematic representation of the DNA origami nanofork having a DNA bridge that is 90 nt long. **(B)** AFM and TEM images of the DNA origami nanofork. The sizes of the close-up AFM and TEM images on the lower left are both approx. 90 nm × 100 nm. **(C)** Two differently coated nanoparticles can be attached selectively via DNA hybridization to the two different sequences of DNA capture strands on the arms and the bridge of the DNA origami to form DONA structures. A side-view and a top-view scheme of the assembled DONA structures is shown. The position of an analyte molecule attached to the DNA bridge is illustrated as a green glow. The DNA hybridisation of nanoparticles and DNA origami in the "zipper" configuration is shown in the insets. **(D)** Representative TEM image of an assembled smaller gap size Au DONA (more examples shown in Fig. S2), along with distributions of gap sizes determined from TEM images of smaller and larger gap size DONAs with an average gap size of 1.17 and 1.40 nm, respectively. The number of the counted DONAs *N* was 109 and 95 for the smaller and larger gap size, respectively.

The nanoforks are characterized by atomic force microscopy (AFM) and transmission electron microscopy (TEM) as shown in Fig. 1B. The images show clearly the successful formation of the

nanoforks including the DNA bridge. In the zoomed-in AFM image the lower part of the base of the DNA origami fork appears elevated, which corresponds to the additional rows of DNA double helices that are also shown in the scheme of the DNA origami structure. The nanoforks are then hybridized with Au or Ag nanoparticles of 60 nm diameter to form the DONAs (Fig. 1C). For optimal SERS measurements a narrow gap between the nanoparticles and precise placement of target molecule therein is required to establish a strong SERS signal enhancement. Two different gap sizes are considered during the experiments, where the gap size is adjusted by adding extra 3 nt spacer sequence between the thiol-group and the segment of the sequence binding to the coating strand (see methods). The larger gap size was used to better accommodate proteins in the gap. We have measured the gap distance of the Au DONA structures containing the short and long coating sequences by TEM, and a typical TEM image of a short coating strand DONA is shown in Fig. 1D, along with a histogram of gap sizes. The most probable gap distance is found to be 1.17 nm and 1.4 nm for the short and the long coating strand, respectively. As the DNA origami nanofork itself is not properly visible in the TEM images (see SI), we confirmed the binding of two differently coated 40 nm AuNPs by separately hybridizing each AuNP to the DNA origami nanofork and characterizing the binding in AFM (Fig. S3). Here, we chose the 40 nm particles to allow a direct visualization of the nanofork. The dimensions of the nanofork are set as such that 60 nm AuNPs cover the fork in a way that the bottom of particles and the nanofork are on the same level. The use of the 60 nm AuNPs throughout the study is partly due to the fact that the bottom of the particles and the nanofork are levelled so that the bottom of the fork is barely touching the substrate in a DONA assembly, which should minimize some of the bending or shear forces exerted by the nanoparticles.

In order to further analyse and optimize the nanofork structure we have performed molecular dynamics simulations using the coarse-grained model oxDNA2.(*16, 17*) The oxDNA model is ideally suited to analyse the effect of bridge length on the distance of the two DNA arms and the general displacement and fluctuation of the DNA bridge, which is important for the precision of the placement of target molecules. We simulated the nanofork with bridge lengths of 120 nucleotides (nt), 90 nt as

well as no bridge. Fig. 2A shows sides and top views of an equilibrated conformation of the DNA origami fork model with a 90 nt bridge, which confirms the overall rigidity of the structure. Fig. 2B shows the probability distributions of the distance between the tips of the two DNA arms (dotted lines). The probability distribution is very broad when no bridge is present, with a maximum around 35 nm, which is slightly shorter than the nominal distance of 40 nm shown in Fig. 1A. With a long bridge of 120 nt, the maximum of the probability function is shifted to 45 nm. With a shorter bridge of 90 nt, the distribution gets narrower with a most probable distance of 40 nm, corresponding to the designed value. An analysis of AFM images of corresponding nanofork samples yields results that match the simulations (Fig. 2B, solid lines, and Figs. S4 and S5). For further experiments we have chosen a bridge length of 90 nt. The simulations also allow to estimate the thermal variation of the centre of the bridge along the plane of the nanofork (Fig. 2C). The plot shows that a shorter DNA bridge increases the stiffness of the bridge, and that for the 90 nt bridge a full-width at half maximum (FWHM) of 3.14 nm is found, indicating the precision with which target molecules placed in the bridge could be located at the plasmonic junction.

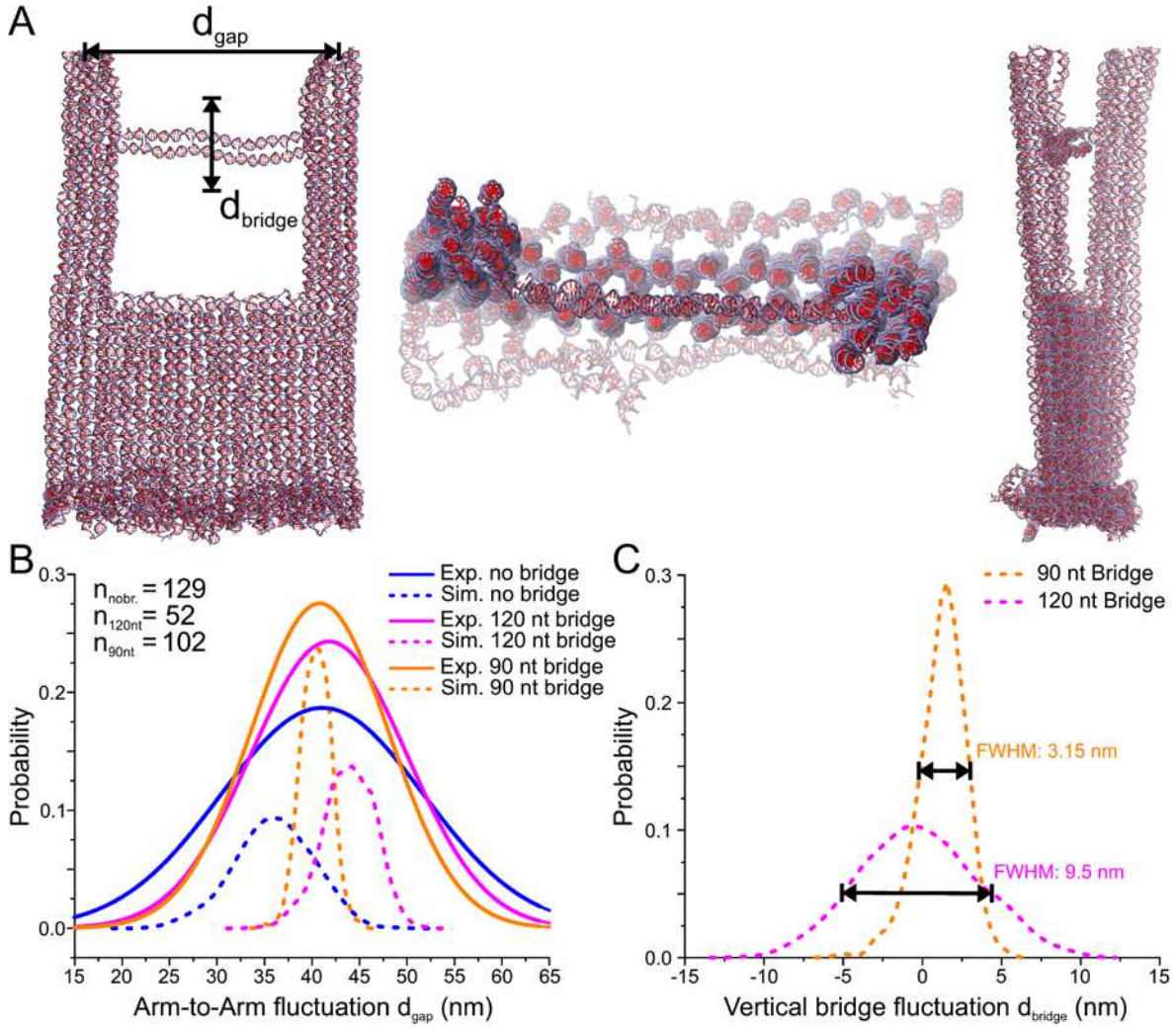

Fig. 2. Coarse-grained oxDNA model of the DNA origami nanofork. (A) Snapshots of two side views and one top-view of the nanofork with 90 nt DNA bridge as simulated using the oxDNA model. **(B)** Plot of the simulated probability distribution of distance between the tips of the two arms and comparison with experimental values obtained from AFM images (for no bridge, 90 nt and 120 nt bridge, the maxima are 41.13 nm, 40.82 nm and 41.84 nm, respectively). The number of nanoforks analysed by AFM is given in the inset. **(C)** Plot of the simulated probability distribution of the flexibility of the centre of a 90 nt and a 120 nt DNA bridge in respect to the straight bridge position, with the maxima at 1.56 nm and -0.6 nm, respectively.

To test the performance of the DONAs for SM SERS we have placed single dye molecules (TAMRA, Cy3.5 and Cy5) at the centre of the DNA bridge using dye-modified staple strands and then assembled Au and Ag DONAs (see Methods and Table S1). In general, to achieve single molecular sensitivity, a

system should produce electric (E) field enhancements in the order of 10^9 - 10^{12}. To investigate this, we calculated the field enhancement (FE) in the gap between the particles with 60 nm diameter as a function of wavelength using the finite difference time domain (FDTD) method (see Methods and SI for details). We have considered different gap sizes ranging from 1.2 nm (corresponding to the mean gap size found in TEM images) to 3.5 nm as shown in Fig. 3A for Au and in Fig. 3B for Ag dimers. The data in Fig. 3Aa and 3B allow for an analysis of the SERS signal enhancement of nanoparticle dimers with different gap sizes at specific Raman excitation wavelengths and in respect to the most common excitation lines used in Raman spectroscopy (*i.e.* 785 nm, 633 nm, 532 nm and 488 nm). Although the highest FE is predicted for the narrowest gap size (1.2 nm) around 736 nm for the Au dimer, the FDTD simulations indicate that an excitation at 633 nm for Au dimers is still advantageous because dimers with different gap sizes give rise to a SERS signal enhancement of 10^9 or higher at this wavelength. For example, the FE at 633 nm excitation wavelength is 255 for a 1.2 nm gap and 312 for a 2.5 nm gap, corresponding to a SERS signal enhancement of around 4.2×10^9 and 9.5×10^9, respectively, using the E^4 approximation.(*40*)

Besides the plasmonic enhancement, the SERS signal depends also on the optical properties of the analyte molecules, *i.e.* their optical absorption. The SERS signal can either be further enhanced by the resonance Raman effect by matching the molecule's optical absorption with the LSPR,(*41*) or non-resonant molecule excitation can be used to avoid photobleaching.

Fig. 3C shows examples of SM SERS spectra of TAMRA, Cy3.5 and Cy5, which are obtained from Au DONAs excited at 633 nm and Ag dimers excited at 532 nm (see Methods and Figs. S6-S9). The black spectra (Fig. 3C) are reference spectra of the respective dyes (see Methods, Figs. S10 and S11 for SERS spectra and S12 for the absorption spectra). Excitation at 532 nm as used for Ag dimers results in an SM SERS signal with considerably higher signal-to-noise ration than in previous SM SERS studies.(*20*) Interestingly, when using 633 nm excitation for the corresponding Au DONA, SM SERS of TAMRA can be measured, although TAMRA does not absorb at 633 nm and therefore resonant Raman contributions can be excluded in this case. This indicates that the plasmonic field enhancement at 633

nm is indeed strong enough to detect a single molecule under non-resonant conditions, which is also supported by our FDTD simulations. The same behaviour is observed for Cy3.5, which can be excited by the 532 nm laser, but not sufficiently by the 633 nm laser. Nevertheless, strong and characteristic single-molecule SERS spectra are obtained for both, Au and Ag DONAs. The strongest absorption of Cy5 is observed at around 650 nm (Fig. S12), close to the 633 nm excitation used for the Au dimers. Consequently, a strong and characteristic single molecule SERS spectrum[28] is obtained for Cy5 using the Au DONAs.

The presented dye spectra include also several peaks that cannot be attributed to dye spectra such as the peak at 1608 cm^{-1} in the case of the Tamra-Ag-DONA in the Fig. 3C. The most probable source of these peaks is the DNA from the DNA coating layer and the DNA bridge,(*42*) which is inherently present in the system. To rule out that the observed spectra would originate from DNA and not from the dyes, we performed control measurements using nanoforks with pure DNA bridges (i.e. no dyes) and averaged several spectra for both the dyes (see Fig. S13) and the pure DNA bridges (see Figs. S13, S14 and S15). Although in some cases the pure DNA-bridge DONAs contained similar peak as in the case of the dyes, the average spectra did not resemble any identifiable DNA fingerprint spectra, indicating that these peaks appear only randomly and we are not systematically measuring the surrounding DNA. In contrast, the average DONA-dye spectra displayed clearly the characteristics peak of the set dyes and thus the dye characteristic peaks observed in the Fig. 3C can be attributed to the dyes. Therefore, the success of SM SERS measurements using different dyes, nanoparticle species and excitation wavelengths demonstrate the strength and versatility of DONAs, *i.e.* the ability to tune the plasmonic properties according to the needs of the molecular systems to be investigated.

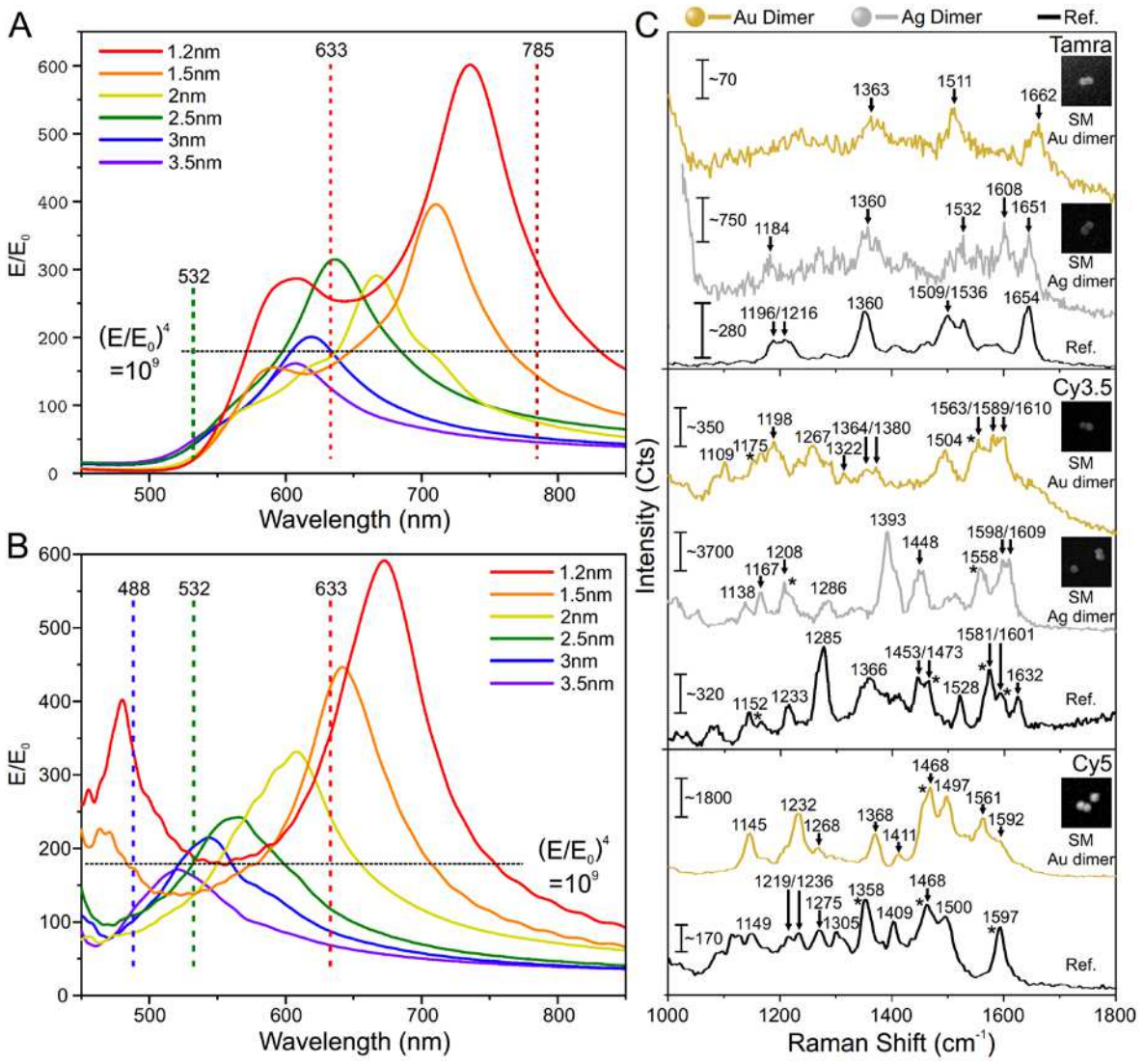

Fig. 3. FDTD simulations of DNA coated Au and Ag dimers and single-molecule SERS spectra of different dyes. The dashed line in a. and b. indicates a field enhancement of 10^9 that is assumed to be the requirement for single molecule detection. **(A)** FDTD simulations of the E-field enhancement of a Au dimer consisting of DNA coated 60 nm diameter particles on a silicon substrate. **(B)** FDTD simulations of the E-field enhancement of a DNA coated Ag dimer consisting of 60 nm diameter particles on a silicon substrate. **(C)** SM SERS spectra of TAMRA, Cy3.5 and Cy5 obtained using Au and Ag DONAs (Cy5 was measured only using Au DONAs). The inset shows SEM images of the specific DONAs, from which the SM SERS spectra have been obtained. The size of the inset SEM images is 450 x 450 nm.

Typically, SM SERS spectra show strong fluctuations of the signal intensity with time. Fig. 4 presents a continuous time series SERS measurement of a Au DONA with a TAMRA dye at 633 nm excitation over the course of 120 seconds recorded using combined dark field and Raman microscopy (see Methods and Figs. S16 and S17). The characteristic signals of TAMRA at 1654 cm^{-1}, 1537 cm^{-1} and 1509 cm^{-1} can be clearly identified, while additional signals attributed to DNA are also observed. The characteristic Raman bands can be observed over several minutes, indicating that no photobleaching of the dye occurs, which is attributed to the fact that TAMRA does not absorb the 633 nm light of the excitation laser. The signal intensity steadily decreases over a time course of several minutes, while the reference signal (Si at 520 cm^{-1}) remains rather constant (Fig. S18). This effect could be due to a soldering of the nanoparticles during the constant laser excitation(*43*) or the DNA structure is damaged or disintegrated possibly due to plasmonic heating.(*44*) On a shorter time scale (as displayed in Fig.4), clear fluctuations of the signals are observed, which correspond to SERS blinking.(*4, 45–47*) One example are the bands at 1537 and 1509 cm^{-1}: For the first 70 s, the band at 1537 cm^{-1} is clearly stronger than the band at 1509 cm^{-1}, while the band at 1537 cm^{-1} almost disappears between 70 s and 100 s, and subsequently the original intensity ratio is restored. Both bands are assigned to C-C stretching vibrations,(*48*) the intensity of which varies according to thermal movements of the molecule within the SERS hot spot, giving rise to SERS blinking. Furthermore, it should be noted, that the band expected

at 1360 cm^{-1} for TAMRA appears either very weakly during the time series measurements, or it is shifted to 1347 cm^{-1}, e.g. due to the vibrational Stark effect.(*49*)

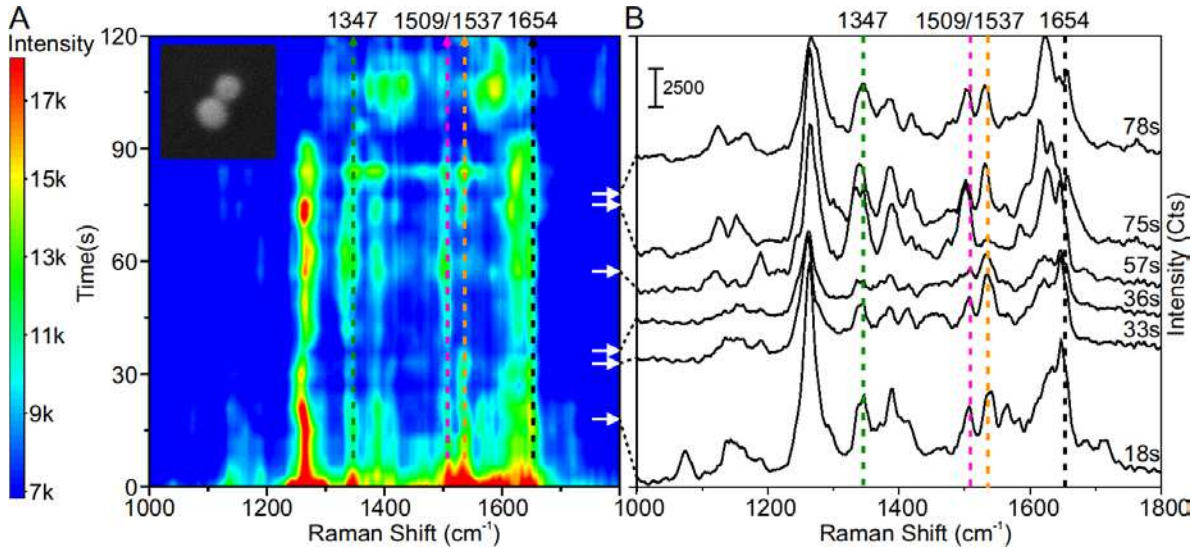

Fig. 4. Single-molecule SERS time series measurements of TAMRA. (A) Time vs Raman shift contour plot for a single TAMRA molecule. The dotted lines indicate the main TAMRA peaks (1654, 1537, 1509). The dotted green line indicates a band at 1347, which can be either a shifted TAMRA band or a DNA peak. The white arrows indicate different times at which the SERS spectra shown in B are extracted. The size of the inset image is 500 nm x 500 nm. **(B)** Full single TAMRA spectra extracted from the contour plot at 48, 63, 66, 87, 105 and 108 s. The same TAMRA bands are indicated with lines as in a.

After demonstrating the potential of DONAs to measure single dye molecules even under non-resonant conditions, we further extend our study to highlight the whole potential of DONAs to directly measure single protein molecules by SERS. This can be achieved with different coupling schemes exploiting either non-covalent or covalent binding of proteins. Here, we have used the heme proteins cyt c and HRP as model systems to demonstrate their direct, label-free and non-resonant single-molecule SERS detection using DONAs (Fig. 5). Cyt c is found in the inner membranes of mitochondria and is involved in biological electron transfer processes, while HRP is involved in oxidation processes.(*50, 51*) Heme proteins strongly absorb at around 420 nm (Soret or B band) and 550 nm (Q

band),(*52*) however, we use the 633 nm excitation laser for the single molecule measurements, which is non-resonant with the heme proteins. In this way, not only the heme prosthetic group is visible in the spectra, but also the amino acid part of the proteins can be directly detected.

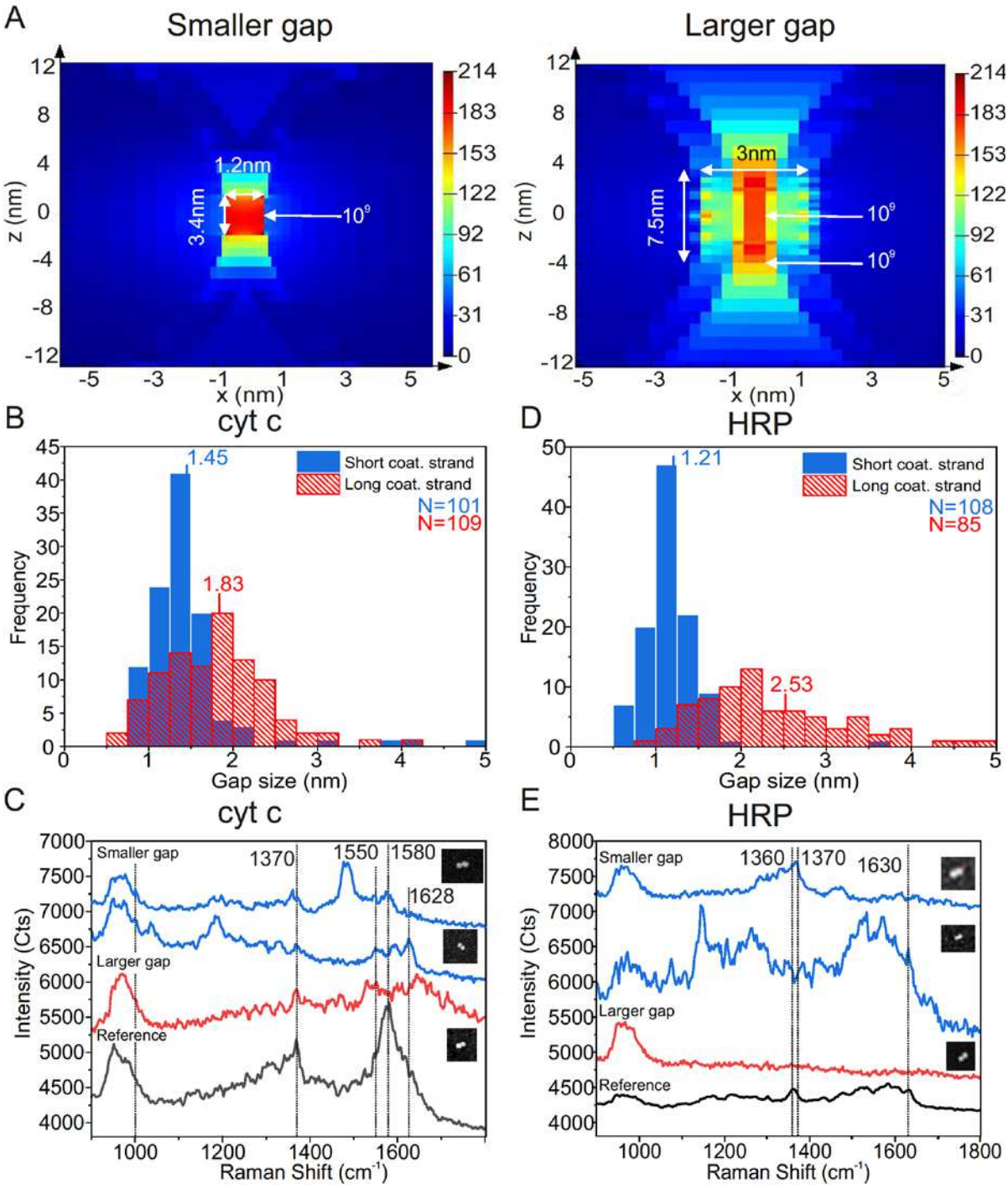

Fig. 5. Single-molecule SERS measurements of cytochrome c (cyt c) and horseradish peroxidase (HRP). (A) Field enhancement plots of the DONA Au dimers, when the gap size is 1.2 nm (smaller gap) and 3 nm (larger gap). **(B)** Distributions of the smaller and larger gap sizes determined from TEM images of cyt c with the average gap sizes of 1.45 nm and 1.83 nm, respectively. The number of counted dimers *N* was 101 and 109 for the smaller and larger gap, respectively. **(C)** SM SERS spectra of cyt c using Au DONA structures and 633 nm excitation. **(D)** Distributions of the smaller and larger gap sizes determined from TEM images of HRP with the average gap sizes of 1.21 nm and 2.53 nm. The number of counted dimers *N* was 108 and 95 for the small and large gap, respectively. **(E)** SM SERS spectra of HRP using Au DONA structures and 633 nm excitation. The insets in C and E show SEM images of the specific DONAs, from which the SM SERS spectra have been obtained. The sizes of the SEM images are from top to bottom 360 × 280 nm, 360 × 420 nm, 300 × 360 nm and 240 × 240 nm 360 x 420 nm 300 x 300 nm, respectively.

For the non-covalent, but specific binding of cyt c to the DONAs, a 4-pyridine moiety (*53*) is coupled via an amide bond and a C5 linker to a staple strand at the centre of the DNA bridge (the sequence shown in Table S1). HRP is covalently coupled to the NHS ester group of a Sulfo-SMCC cross linker via a lysine residue. The maleimide group of the cross linker is then bound to a thiolated staple strand (Table S1), which in turn is incorporated into the DNA bridge of the DNA origami nanofork (the binding schemes of cyto c and HRP are shown in Fig. S19). Both, cyt c and HRP are bound to the DNA origami nanofork prior to the binding of the 60 nm Au nanoparticles. For synthesis of DONAs with smaller and larger gap sizes, we utilized the same particle coating sequences as in the case of dyes and similar sequences with added 3nt spacers at the thiol-end, respectively. The reason for this is two-fold: the benefit for having a smaller gap size is the higher EF as demonstrated in Fig. 2, but the physical size of the protein is larger than the dye and thus it would be more beneficial to increase the hot spot size to fully incorporate the larger molecules. Fig. 5A shows simulations of the field enhancement distributions within the interparticle gaps for two different minimal gap sizes (1.2 nm and 3.0 nm). Based on the simulations, the effective hot spot, i.e. the volume where a field enhancement of 10^9 is still achieved, is roughly 11 nm^3 for the 1.2 nm gap size and approximately 27 nm^3 for the 3 nm gap

size. For the larger gap size the volume enclosing a signal enhancement of ≥ 10^9 along the dimer axis, which is available for a protein is approximately 133 nm^3. This would suggest that increase in the gap size should overall benefit the incorporation and detection of larger proteins. The volume of cyt c is approximately 14 nm^3,(*54*) while the volume of HRP is about 41 nm^3,(*55*) indicating that cyt c is small enough to be completely affected by a signal enhancement sufficient for single molecule detection in the larger gap hot spot, while only part of the HRP can be localized in the volume of highest signal enhancement.

Fig. 5B and 5D show the gap distances of DONAs with shorter and longer coating strands containing cyt c or HRP, respectively, as determined from TEM images. Accordingly, even for the shorter coating strands the gap sizes increase when the proteins are present compared to the dye containing DONAs shown in the Fig. 1D. Apparently, the presence of the proteins prevents the nanoparticles from coming closer, which is another indirect proof of successful positioning of proteins into the hot spot. With longer coating strands the DONAs offer more flexibility and the gap size increases on average from 1.45 nm (shorter coating strands) to 1.83 nm for cyt c, and from 1.21 nm to 2.53 nm for HRP, while at the same time the gap distributions become broader. Examples of single-molecule SERS spectra of cyt c and HRP for the shorter and longer coating strand DONAs (blue and red spectra, respectively), recorded at 633 nm excitation are shown in Fig. 5C and 5E along with the corresponding SEM images of Au dimers and a reference spectrum (black spectra, see also Figs. S20 and S21). The reference spectra were obtained from clusters of 60 nm Au nanoparticles with unspecifically bound cyt c or HRP, respectively (see Methods). The characteristic band appearing around 1370 cm^{-1} in both the cyt c and the HRP spectra is assigned to the stretching vibration of the porphyrin ring (ν_4) of the heme group indicating the oxidation state of the central iron ion (Fe^{3+}).(*52, 56*) The strong signal around 1580 cm^{-1} appearing in the cyt c spectra is assigned to the ν_{19} band, the exact position of which is strongly dependent on the spin state of the central iron ion.(*52*) The band at 1628-1630 cm^{-1} is due to the ν_{10} band, the spectral position of which is also indicative of the oxidized form of cyt c. In general, characteristic cyt c signals can be observed for both the smaller and larger gap sizes, which supports

the general conclusion that also larger gap sizes can lead to signal enhancements sufficient for single-molecule detection. But we find a better spectral reproducibility for the shorter gap size suggesting a more pronounced conformational flexibility in the case of larger gap sizes. Apart from the signals arising from the heme unit of cyt c, the vibrational ring-breathing mode of the amino acid phenylalanine (Phe) can also be clearly distinguished at 1001 cm^{-1},(*57*) but interestingly only for the smaller gap size DONAs. Cyt c possesses four Phe residues, and the possibility to detect this band in a single cyt c molecule by SERS using DONAs indicates the high sensitivity of the method. Also for HRP characteristic SERS signals can be clearly detected in the case of DONAs with shorter coating strands. In addition to the ν_4 band at 1370 cm^{-1} (which is broader in the reference spectrum with a shift to smaller wavenumber because both oxidation states appear in the reference) also the oxidation state marker at 1630 cm^{-1} (ν_{10}) is visible, indicating the presence of Fe^{3+}.(*52*) With HRP we were not able to collect single molecule SERS spectra for the larger gap sizes, which might be an indication for a non-sufficient signal enhancement due to the larger gap sizes. Nevertheless, single-molecule SERS spectra of HRP could be detected for the smaller gap size DONAs.

Lastly, although we purify the solution from excess of free proteins after binding them to the forks, we have a minute amount of proteins left in the solution, which could bind unspecifically to the AuNPs or to the nanoforks. To test the possibility of contributions by unspecifically bound proteins to the measured SM-SERS protein spectra, we repeated the same sample fabrication process using nanoforks without any capture mechanism (i.e. no thiol or pyridine in the bridge). Interestingly, the DONA structures for each protein did not exhibit any spectra that could be identified as either cyt c or HRP (Figs. S22 and S23) proving that the SERS spectra in the Fig. 5 originate from a single protein in the bridge rather than from any unspecifically bound protein.

Discussion

In conclusion, the newly designed 3D DNA origami nanofork has successfully been demonstrated for its suitability to assemble both nanoparticles and complex analyte molecules with nanoscale precision for SM SERS measurements. OxDNA simulations were employed to assess the structural dynamics of

the nanofork and to choose the most suitable bridge length. The DNA bridge connecting the two arms of the nanofork allows for precise positioning of the target analyte in between the assembled nanoparticles of Au and Ag. This produces SERS hot spots in the scale of few nanometers, creating high enough field enhancement to enable label-free detection of single small molecules and even proteins (cyt c and HRP) via SERS, even at larger gap sizes around 2.5 nm. Importantly, the flexible integration of either Au and Ag nanoparticles supports SM SERS measurements both in resonant and non-resonant conditions. Time-dependent SM SERS of TAMRA under non-resonant conditions shows spectral blinking but no significant photobleaching, strikingly reflecting the single-molecular SERS behaviour. The experimental findings are supported by FDTD simulations that predict field enhancements high enough for single molecule measurements under non-resonant conditions. DNA origami is a remarkable technique that offers options to achieve control over single molecular entities, thereby enabling novel types of nanomachines.(*18, 58*) Here, we used this principle to build a platform for the direct, chemically-specific and label-free optical detection of single small molecules and single proteins. This opens new potential to study biomolecular reactions at the single molecule level. One critical aspect of our design is the ability to generate arbitrary dimer compositions of any arbitrarily sized and shaped nanoparticles. The DONA structures could be used to monitor enzymatic action in different environments, perhaps even for multi-enzyme reaction cascades. At the same time, sensing of single small molecules represents one of the greatest challenges in analytical chemistry which could be achieved with the present DONA structure. This therefore opens a way to study single reaction intermediates which could prove invaluable for understanding chemical reaction pathways.

Materials and Methods

DNA origami nanofork folding and purifications

The staple strands used for the assembly of the DNA origami nanofork are shown in Table S2. Depending on the experiment, some strands were substituted with the modified versions of the same strand (see Table S1). The folding solution was made by mixing 10 µl of 10x buffer (10xTAE, 150 mM $MgCl_2$), 67.5 µl of Millipore water, 20

µl of staple solution (the concentration of individual staple = 0.497 µM) and 2.5 µl of the scaffold (m13mp18, 0.1 µM). During folding, the ratio between staples and the scaffold is 40:1. The folding solution was heated to 80°C and then cooled down to 20°C over 15 h timespan. The solution was purified from excess oligos using 100 kDa centrifugal filters (Amicon, Ultracel, Centrifugal filter, 100 kDA): the DNA origami solution (100 µl) was added to the filter and 400 µl of Millipore water was mixed in, the filter was spun in 4700 rcf for 5min, the filtrate was discarded and 450 µl of Millipore water was added. The centrifugation was repeated 3 times and the dead volume from the filter was finally recovered. The concentration of TAE and $MgCl_2$ was adjusted to 1x and 5 mM, respectively. A UV-vis spectrometer was used to measure the DNA concentration of the final solution that was used to calculate the DNA origami concentration.

Nanoparticle coating protocols

Gold (Au nanosphere NanoXact, citrate coated, 60 nm, 2.4×10^{10} particles/ml) and silver (Ag nanosphere NanoXact, citrate coated, 60 nm, 1.9×10^{10} particles/ml) nanoparticles were purchased from nanoComposix (4878 Ronson Ct Ste J, San Diego, USA). The DNA strands in the table S2 were acquired from Sigma Aldrich (Sigma-Aldrich Chemie GmbH, Munich, Germany). Tris(2-carboxyethyl)phosphine (TCEP) was purchased from RIZ Biochem.

The gold nanoparticles were coated using a modified salt aging method, whereas the coating for silver nanoparticles was done using a pH altering method.(*59*) For AuNPs, 400 µl of 60 nm AuNP stock solution were centrifuged once (2900 rcf, 5 min), the supernatant was removed and the volume was adjusted to 26.5 µl by MilliQ water. The disulphide bonds in the DPTA-modified coating strands were pre-cleaved using TCEP: 4 µl of the coating strand solution (100 µM) was mixed with 1µl of TCEP (100 mM) and incubated at RT for 10 min. The 5 µl of cleaved DNA strand solution and 3.5 µl of 0.2 % SDS was added to the AuNP solution and incubated 40 min to 1h and at 40 °C. After the incubation, the concentration of NaBr was gradually, in stepwise manner increased to 300 mM using initially 400 mM NaBr buffer and then 1 M buffer, where after each step the solution was incubated for 10 min at 40 °C: initial 4 steps were 1.7 µl (400 mM), the next two 2.1 µl and 2.3 µl (400 mM), followed by 3x 2.3 µl and 1 M and finally 6.5µl and 1 M. After the NaBr addition, 1x TAE and 5 mM $MgCl_2$ was added twice (6 µl and 6.6 µl) in similar stepwise manner. Finally, the excess coating strands were purified by centrifugation: the sample was spun down using 2900 rcf and 5 min, supernatant was removed and buffer added.

During the first two round of centrifugation, 1xTAE, 5 mM $MgCl_2$ and 0.02 % SDS buffer was used and during the final two rounds, the buffer was switched to 1xTAE and 5 mM $MgCl_2$.

For silver particles, 400 µl of the 60 nm AgNP solution was centrifuged once (2900 rcf, 5 min), the supernatant was removed and the volume was adjusted to 26.5 µl by MilliQ water. The coating strands were cleaved similarly as in the case of AuNPs using TCEP. 3.5 µl of 0.2 % SDS and 5 µl of DNA solution were added to the AgNP solution and incubated for 40 min at RT. Then the pH of the solution was adjusted close to 3 by adding 1.4 µl of 0.5 M TSC (pH 3, adjusted using HCl) to the mixture. After 3 min incubation at RT, NaCl (1 M) was added in stepwise manner until the final NaCl concentration of the AgNP solution was 0.3 M: 2 µl of NaCl was added 6 times followed by final addition of 3.6 µl, where in-between additions the solution was rapidly vortexed and let stand still for few seconds. The particles were incubated for 5 min after the final addition of the NaCl, and purified similarly as the AuNPs.

DONA assembly, gel electrophoresis purifications

DONAs were fabricated by mixing DNA origami nanoforks with two different 60 nm AuNP/AgNP batches, where for the shorter gap size particles one particle is coated with T_{28} sequence and the other with $(GTT)_8T_4$ sequence. For the larger gap size particles, the sequences were $T_{28}GGT$ and $(GTT)_8T_7$, respectively. All materials were dissolved in 1xTAE and 5 mM $MgCl_2$ buffer. The ratio of NP-T_{28}: NP-$(GTT)_8T_4$: nanofork is 1.5 : 1.5 : 1 and the final concentration of nanoforks is between 0.1 and 0.2 nM. The ratio was the same for the longer sequences. The mixture was heated in a thermocycler to 40 °C and then cooled down to 20 °C in 3.5h timespan. In some cases such as nanoforks with dyes, agarose gel electrophoresis was used to extract the dimers from the final product. Shortly, samples were run in 1% agarose gel made in 1xTAE and 5 mM $MgCl_2$ for 60 min using 80 V. The dimer band was cut out of the gel and the dimers were squeezed out using two microscope slides.

TEM imaging of DNA origami nanoforks and DONAs

All samples were imaged in JEOL JEM 1011 transmission electron microscope (JEOL, Akishima, Tokyo, Japan) equipped with Olympus MegaView G2 camera and using 80kV acceleration voltage. In the TEM imaging, copper grids containing 1 nm carbon layer on top of 10 nm formvar film (EFCF400-Cu-50, Science Services GmbH, Unterhachinger Straße 75, Munich, Germany) were used. To characterize the dimer gap sizes, the DONA solution was deposited on a TEM grid. For DONA deposition, no plasma-treatment was required whereas, for nanoforks, the TEM grids were plasma-treated for 15 s using Diener Electronic Zepto plasma cleaner before deposition of

the DNA origami and the staining. In the case of DONAs, 3 µl of DONA solution was pipetted to the grid and incubated for 2-3 min. The excess solution was blotted away and 3 µl of staining solution was added. After 2 min incubation, the excess staining solution was blotted away and the film was washed twice by adding 3 µl of Millipore water to the grid and blotting away the excess liquid. The grid was let to dry in ambient conditions.

In the case of DNA origami nanofork, after the plasma treatment, roughly 3 µl of DNA origami solution was pipetted on a grid and incubated for 5 min. The magnesium and fork concentrations were 20 mM and 0.6 nM, respectively. The excess solution was blotted away and 3 µl of the same staining solution was added. After 2 min incubation, the excess solution was blotted away and the sample was left to dry in ambient condition without any washing. Fig. S24 contains extra images of the DNA origami nanoforks.

Sample preparation for SERS, SERS measurements, SEM imaging and SERS-SEM correlation

DONAs were deposited on a 7 mm x 7 mm silicon chip labelled with a scratch-marker. A diamond cutter was used to draw a cross-shape on the chip, the surface was scrubbed clean from dust in acetone solution using a cotton stick and cleaning was finalized by sonicating the chip in ethanol solution for 30 s. The clean chip was plasma-treated for 10 min. For the deposition, the magnesium concentration of DONA solution was adjusted to 50 mM, the solution was pipetted to plasma-treated silicon surface and incubated for roughly 1.5 h. The chip was washed with ethanol-water solution (1:1 ratio) and blown dry.

A Witec Alpha 300 Raman microscope was used in the measurements (Witec, Ulm, Germany). For the 488 and 532 nm measurements a grating spectrograph (Blaze 500, grating 600 gr/mm) equipped with Andor DV401-BV CCD-camera was used, and for the 633 nm measurements a spectrograph (Blaze 750, grating 600 gr/mm) equipped with Andor DU401A-BR-DD-352 CCD-camera. The estimated spot sizes were 1.32 µm, 1.44 µm and 1.72 µm for 488 nm, 532 nm and 633 nm, respectively. Raman maps were acquired using varying laser power densities and integration times per point (see SI). After a Raman measurement, the Raman map area was imaged using SEM (Thermo Fisher Phenom ProX Desktop SEM or FEI Quanta 250) where the scratch-markers acted as reference points to identify the area scanned with the Raman microscope. For the dye references, particles coated with dye-T_{28} oligos were deposited on a silicon surface and point spectra were measured using 532 or 633 nm laser (see SI for more details). For protein samples, the proteins were incubated with the nanoparticles before to adsorb them to the particle surface and cause aggregation. Then the aggregates were deposited on a

silicon surface and point measurements were performed using the 633 nm laser and 300 μW (200 μW) laser power and 8 s (12 s) integration time for cyt c (HRP).

FDTD simulations

A detailed overview of the FDTD simulations can be found in the SI. In brief, we used the Lumerical FDTD Solutions software (v8.19.1584). The model included two gold or silver spheres (refractive index from Johnson and Christy)(*60*) surrounded by 1.12 nm DNA layer (refractive index 1.7)(*25*) and on top of a silicon substrate (refractive index from (*61*)) with 3 nm silicon dioxide (refractive index 1.44) on top of the Si. The DNA layer thickness was measured using AFM (Figs. S25 and S26). The model is presented in Fig. S27. Here, we are omitting the bridge and the DNA origami nanofork from the framework. The medium was defined as air. The distance between gold spheres was varied according to the measured distance from Fig. 1 (from 1.2 nm to 3.5 nm), where a water layer was added between DNA layers in the case of 2.5 and 3 nm particle-to-particle distances. The E field distributions were calculated and the field maximum around the gap region was recorded. To solve the E_0 case, we removed the DNA layers and the metal spheres. Electric field polarizations along the gap (the gap mode) and perpendicular to gap (the off-gap mode) were considered. The results show that the electric field is highly localized within the gap region in the case of the gap mode and the off-gap mode excitation results mainly in plasmonic mode that resembled single particle dipole excitation (Figs. S28-S32). The volumes of the 1.2 nm and 3 nm gap size hot spots were calculated from Fig. S33.

OxDNA simulations

We performed Langevin molecular dynamics simulations for the three nanofork structures considered (90 nt, 120 nt and no bridge) using the coarse-grained DNA model oxDNA2,(*16, 17*) parametrized to reproduce mechanical and thermodynamic experimental properties of DNA. The initial oxDNA configurations were obtained converting the caDNAno files with the tacoxDNA package.(*62*) The caDNAno model of the nanofork is shown in Fig. S34 . Simulations were carried out with the LAMMPS software implementation.(*63*) The temperature was set to T = 300 K and the monovalent salt concentration to 1 M. Each system was simulated for about 2 x 10^6 simulation time units, for a total of 2000 configurations sampled.

Acknowledgment

We thank Sibylle Rüstig for assisting in TEM imaging. **Funding:** This research was supported by the European Research Council (ERC; consolidator grant no. 772752). **Author contributions:** IB conceived the study, KT and AM prepared and characterized DONAs, KT did the TEM imaging and dye measurements and performed FDTD simulations, AM did sample preparations and measurement involving cyt c, YK did sample preparations and measurement involving HRP, AS performed OxDNA simulations, and all authors analysed the data and contributed to manuscript writing. **Competing interests:** The authors declare no competing interests.

References:

1. S. A. Claridge, J. J. Schwartz, P. S. Weiss, Electrons, photons, and force: quantitative single-molecule measurements from physics to biology. *ACS Nano* **5**, 693–729 (2011).
2. W. E. Moerner, David P. Fromm, Methods of single-molecule fluorescence spectroscopy and microscopy. *Rev. Sci. Instrum.* **74**, 3597 (2003).
3. N. Pavliček, L. Gross, Generation, manipulation and characterization of molecules by atomic force microscopy. *Nat. Rev. Chem.* **1** (2017).
4. A. B. Zrimsek, N. Chiang, M. Mattei, S. Zaleski, M. O. McAnally, C. T. Chapman, A.-I. Henry, G. C. Schatz, R. P. van Duyne, Single-Molecule Chemistry with Surface- and Tip-Enhanced Raman Spectroscopy. *Chem. Rev.* **117**, 7583–7613 (2017).
5. R. Pilot, R. Signorini, C. Durante, L. Orian, M. Bhamidipati, L. Fabris, A Review on Surface-Enhanced Raman Scattering. *Biosensors* **9** (2019).
6. J. Langer, D. Jimenez de Aberasturi, J. Aizpurua, R. A. Alvarez-Puebla, B. Auguié, J. J. Baumberg, G. C. Bazan, S. E. J. Bell, A. Boisen, A. G. Brolo, J. Choo, D. Cialla-May, V. Deckert, L. Fabris, K. Faulds, F. J. García de Abajo, R. Goodacre, D. Graham, A. J. Haes, C. L. Haynes, C. Huck, T. Itoh, M. Käll, J. Kneipp, N. A. Kotov, H. Kuang, E. C. Le Ru, H. K. Lee, J.-F. Li, X. Y. Ling, S. A. Maier, T. Mayerhöfer, M. Moskovits, K. Murakoshi, J.-M. Nam, S. Nie, Y. Ozaki, I. Pastoriza-Santos, J. Perez-Juste, J. Popp, A. Pucci, S. Reich, B. Ren, G. C. Schatz, T. Shegai, S. Schlücker, L.-L. Tay, K. G. Thomas, Z.-Q. Tian, R. P. van Duyne, T. Vo-Dinh, Y. Wang, K. A. Willets, C. Xu, H. Xu, Y. Xu, Y. S. Yamamoto, B. Zhao, L. M. Liz-Marzán, Present and Future of Surface-Enhanced Raman Scattering. *ACS Nano* **14**, 28–117 (2020).
7. H. M. Lee, S. M. Jin, H. M. Kim, Y. D. Suh, Single-molecule surface-enhanced Raman spectroscopy: a perspective on the current status. *Phys. Chem. Chem. Phys.* **15**, 5276–5287 (2013).
8. E. C. Le Ru, P. G. Etchegoin, Single-molecule surface-enhanced Raman spectroscopy. *Annu. Rev. Phys. Chem.* **63**, 65–87 (2012).

9. J.-H. Lee, J.-M. Nam, K.-S. Jeon, D.-K. Lim, H. Kim, S. Kwon, H. Lee, Y. D. Suh, Tuning and maximizing the single-molecule surface-enhanced Raman scattering from DNA-tethered nanodumbbells. *ACS Nano* **6**, 9574–9584 (2012).

10. Rothemund, Paul W. K., Folding DNA to create nanoscale shapes and patterns. *Nature* **440**, 297–302 (2006).

11. H. Dietz, S. M. Douglas, W. M. Shih, Folding DNA into twisted and curved nanoscale shapes. *Science* **325**, 725–730 (2009).

12. K. F. Wagenbauer, C. Sigl, H. Dietz, Gigadalton-scale shape-programmable DNA assemblies. *Nature* **552**, 78–83 (2017).

13. S. M. Douglas, A. H. Marblestone, S. Teerapittayanon, A. Vazquez, G. M. Church, W. M. Shih, Rapid prototyping of 3D DNA-origami shapes with caDNAno. *Nucleic acids research* **37**, 5001–5006 (2009).

14. C. E. Castro, F. Kilchherr, D.-N. Kim, E. L. Shiao, T. Wauer, P. Wortmann, M. Bathe, H. Dietz, A primer to scaffolded DNA origami. *Nature methods* **8**, 221–229 (2011).

15. D.-N. Kim, F. Kilchherr, H. Dietz, M. Bathe, Quantitative prediction of 3D solution shape and flexibility of nucleic acid nanostructures. *Nucleic acids research* **40**, 2862–2868 (2012).

16. T. E. Ouldridge, A. A. Louis, J. P. K. Doye, Structural, mechanical, and thermodynamic properties of a coarse-grained DNA model. *J. Chem. Phys.* **134**, 85101 (2011).

17. B. E. K. Snodin, F. Randisi, M. Mosayebi, P. Šulc, J. S. Schreck, F. Romano, T. E. Ouldridge, R. Tsukanov, E. Nir, A. A. Louis, J. P. K. Doye, Introducing improved structural properties and salt dependence into a coarse-grained model of DNA. *J. Chem. Phys.* **142**, 234901 (2015).

18. K. Tapio, I. Bald, The potential of DNA origami to build multifunctional materials. *Multifunctional Materials* (2020).

19. J. Prinz, B. Schreiber, L. Olejko, J. Oertel, J. Rackwitz, A. Keller, I. Bald, DNA Origami Substrates for Highly Sensitive Surface-Enhanced Raman Scattering. *J. Phys. Chem. Lett.* **4**, 4140–4145 (2013).

20. J. Prinz, C. Heck, L. Ellerik, V. Merk, I. Bald, DNA origami based Au-Ag-core-shell nanoparticle dimers with single-molecule SERS sensitivity. *Nanoscale* **8**, 5612–5620 (2016).

21. C. Heck, J. Prinz, A. Dathe, V. Merk, O. Stranik, W. Fritzsche, J. Kneipp, I. Bald, Gold Nanolenses Self-Assembled by DNA Origami. *ACS Photonics* **4**, 1123–1130 (2017).

22. C. Heck, Y. Kanehira, J. Kneipp, I. Bald, Placement of Single Proteins within the SERS Hot Spots of Self-Assembled Silver Nanolenses. *Angew. Chem. Int. Ed.* **57**, 7444–7447 (2018).

23. N. Liu, T. Liedl, DNA-Assembled Advanced Plasmonic Architectures. *Chem. Rev.* **118**, 3032–3053 (2018).

24. M. Pilo-Pais, A. Watson, S. Demers, T. H. LaBean, G. Finkelstein, Surface-enhanced Raman scattering plasmonic enhancement using DNA origami-based complex metallic nanostructures. *Nano Lett.* **14**, 2099–2104 (2014).

25. V. V. Thacker, L. O. Herrmann, D. O. Sigle, T. Zhang, T. Liedl, J. J. Baumberg, U. F. Keyser, DNA origami based assembly of gold nanoparticle dimers for surface-enhanced Raman scattering. *Nat. Commun.* **5**, 3448 (2014).

26. S. Simoncelli, E.-M. Roller, P. Urban, R. Schreiber, A. J. Turberfield, T. Liedl, T. Lohmüller, Quantitative Single-Molecule Surface-Enhanced Raman Scattering by Optothermal Tuning of DNA Origami-Assembled Plasmonic Nanoantennas. *ACS Nano* **10**, 9809–9815 (2016).

27. S. Tanwar, K. K. Haldar, T. Sen, DNA Origami Directed Au Nanostar Dimers for Single-Molecule Surface-Enhanced Raman Scattering. *J. Am. Chem. Soc.* **139**, 17639–17648 (2017).

28. P. Zhan, T. Wen, Z.-G. Wang, Y. He, J. Shi, T. Wang, X. Liu, G. Lu, B. Ding, DNA Origami Directed Assembly of Gold Bowtie Nanoantennas for Single-Molecule Surface-Enhanced Raman Scattering. *Angew. Chem. Int. Ed.* **57**, 2846–2850 (2018).

29. G. P. Acuna, F. M. Möller, P. Holzmeister, S. Beater, B. Lalkens, P. Tinnefeld, Fluorescence enhancement at docking sites of DNA-directed self-assembled nanoantennas. *Science* **338**, 506–510 (2012).

30. A. Puchkova, C. Vietz, E. Pibiri, B. Wünsch, M. Sanz Paz, G. P. Acuna, P. Tinnefeld, DNA Origami Nanoantennas with over 5000-fold Fluorescence Enhancement and Single-Molecule Detection at 25 µM. *Nano Lett.* **15**, 8354–8359 (2015).

31. J. Prinz, A. Matković, J. Pešić, R. Gajić, I. Bald, Hybrid Structures for Surface-Enhanced Raman Scattering: DNA Origami/Gold Nanoparticle Dimer/Graphene. *Small* **12**, 5458–5467 (2016).

32. L. Weller, V. V. Thacker, L. O. Herrmann, E. A. Hemmig, A. Lombardi, U. F. Keyser, J. J. Baumberg, Gap-Dependent Coupling of Ag–Au Nanoparticle Heterodimers Using DNA Origami-Based Self-Assembly. *ACS Photonics* **3**, 1589–1595 (2016).

33. P. Kühler, E.-M. Roller, R. Schreiber, T. Liedl, T. Lohmüller, J. Feldmann, Plasmonic DNA-origami nanoantennas for surface-enhanced Raman spectroscopy. *Nano Lett.* **14**, 2914–2919 (2014).

34. R. Chikkaraddy, V. A. Turek, Q. Lin, J. Griffiths, B. Nijs, U. F. Keyser, J. J. Baumberg, Dynamics of deterministically positioned single-bond surface-enhanced Raman scattering from DNA origami assembled in plasmonic nanogaps. *J. Raman Spectrosc.* **205**, 291 (2020).

35. R. Chikkaraddy, V. A. Turek, N. Kongsuwan, F. Benz, C. Carnegie, T. van de Goor, B. de Nijs, A. Demetriadou, O. Hess, U. F. Keyser, J. J. Baumberg, Mapping Nanoscale Hotspots with Single-Molecule Emitters Assembled into Plasmonic Nanocavities Using DNA Origami. *Nano Lett.* **18**, 405–411 (2018).

36. W. Fang, S. Jia, J. Chao, L. Wang, X. Duan, H. Liu, Q. Li, X. Zuo, L. Wang, L. Wang, N. Liu, C. Fan, Quantizing single-molecule surface-enhanced Raman scattering with DNA origami metamolecules. *Science advances* **5**, eaau4506 (2019).

37. B. Ding, Z. Deng, H. Yan, S. Cabrini, R. N. Zuckermann, J. Bokor, Gold nanoparticle self-similar chain structure organized by DNA origami. *J. Am. Chem. Soc.* **132**, 3248–3249 (2010).

38. X. Shen, A. Asenjo-Garcia, Q. Liu, Q. Jiang, F. J. García de Abajo, N. Liu, B. Ding, Three-dimensional plasmonic chiral tetramers assembled by DNA origami. *Nano Lett.* **13**, 2128–2133 (2013).

39. S. Fischer, C. Hartl, K. Frank, J. O. Rädler, T. Liedl, B. Nickel, Shape and Interhelical Spacing of DNA Origami Nanostructures Studied by Small-Angle X-ray Scattering. *Nano Lett.* **16**, 4282–4287 (2016).

40. S.-Y. Ding, E.-M. You, Z.-Q. Tian, M. Moskovits, Electromagnetic theories of surface-enhanced Raman spectroscopy. *Chem. Soc. Rev.* **46**, 4042–4076 (2017).

41. G. McNay, D. Eustace, W. E. Smith, K. Faulds, D. Graham, Surface-enhanced Raman scattering (SERS) and surface-enhanced resonance Raman scattering (SERRS): a review of applications. *Appl. Spectrosc.* **65**, 825–837 (2011).

42. L. Guerrini, Ž. Krpetić, D. van Lierop, R. A. Alvarez-Puebla, D. Graham, Direct surface-enhanced Raman scattering analysis of DNA duplexes. *Angew. Chem. Int. Ed.* **54**, 1144–1148 (2015).

43. A. R. Salmon, M.-E. Kleemann, J. Huang, W. M. Deacon, C. Carnegie, M. Kamp, B. de Nijs, A. Demetriadou, J. J. Baumberg, Light-Induced Coalescence of Plasmonic Dimers and Clusters. *ACS Nano* (2020).

44. R. Huschka, J. Zuloaga, M. W. Knight, L. V. Brown, P. Nordlander, N. J. Halas, Light-induced release of DNA from gold nanoparticles: nanoshells and nanorods. *J. Am. Chem. Soc.* **133**, 12247–12255 (2011).

45. T. Itoh, Y. S. Yamamoto, Recent topics on single-molecule fluctuation analysis using blinking in surface-enhanced resonance Raman scattering: clarification by the electromagnetic mechanism. *Analyst* **141**, 5000–5009 (2016).

46. Y. Kitahama, T. Nagahiro, Y. Tanaka, T. Itoh, Y. Ozaki, Analysis of blinking from multicoloured SERS-active Ag colloidal nanoaggregates with poly-L-lysine via truncated power law. *J. Raman Spectrosc.* **48**, 570–577 (2017).

47. J. R. Lombardi, R. L. Birke, G. Haran, Single Molecule SERS Spectral Blinking and Vibronic Coupling. *J. Phys. Chem. C* **115**, 4540–4545 (2011).

48. A. Jaworska, E. Pyrak, A. Kudelski, Comparison of the efficiency of generation of Raman radiation by various Raman reporters connected via DNA linkers to different plasmonic nano-structures. *Vib. Spectrosc.* **101**, 34–39 (2019).

49. J. M. Marr, Z. D. Schultz, Imaging Electric Fields in SERS and TERS Using the Vibrational Stark Effect. *J. Phys. Chem. Lett.* **4** (2013).

50. I. Bertini, G. Cavallaro, A. Rosato, Cytochrome c: occurrence and functions. *Chem. Rev.* **106**, 90–115 (2006).

51. N. C. Veitch, Horseradish peroxidase: a modern view of a classic enzyme. *Phytochemistry* **65**, 249–259 (2004).

52. A. Rygula, K. Majzner, K. M. Marzec, A. Kaczor, M. Pilarczyk, M. Baranska, Raman spectroscopy of proteins: a review. *J. Raman Spectrosc.* **44**, 1061–1076 (2013).

53. H. Yamamoto, H. Liu, D. H. Waldeck, Immobilization of cytochrome c at Au electrodes by association of a pyridine terminated SAM and the heme of cytochrome. *Chem. Commun.*, 1032–1033 (2001).

54. N. Mirkin, J. Jakoncic, V. Stojanoff, A. Moreno, *Crystal structure of cytochrome C from bovine heart at 1.5 A resolution* (2005) (available at http://dx.doi.org/10.2210/pdb2B4Z/pdb).

55. G. I. Berglund, G. H. Carlsson, J. Hajdu, A. T. Smith, H. Szoke, A. Henriksen, *Structure of horseradish peroxidase C1A compound I* (2002) (available at http://dx.doi.org/10.2210/pdb1HCH/pdb).

56. Y. Kitahama, Y. Ozaki, Surface-enhanced resonance Raman scattering of hemoproteins and those in complicated biological systems. *Analyst* **141**, 5020–5036 (2016).

57. B.-S. Yeo, S. Mädler, T. Schmid, W. Zhang, R. Zenobi, Tip-Enhanced Raman Spectroscopy Can See More: The Case of Cytochrome c. *J. Phys. Chem. C* **112**, 4867–4873 (2008).

58. H. Ramezani, H. Dietz, Building machines with DNA molecules. *Nat. Rev. Genet.* **21**, 5–26 (2020).

59. X. Zhang, M. R. Servos, J. Liu, Instantaneous and quantitative functionalization of gold nanoparticles with thiolated DNA using a pH-assisted and surfactant-free route. *J. Am. Chem. Soc.* **134**, 7266–7269 (2012).

60. P. B. Johnson, R. W. Christy, Optical Constants of the Noble Metals. *Phys. Rev. B* **6**, 4370–4379 (1972).

61. D. T. Pierce, W. E. Spicer, Electronic Structure of Amorphous Si from Photoemission and Optical Studies. *Phys. Rev. B* **5**, 3017–3029 (1972).

62. A. Suma, E. Poppleton, M. Matthies, P. Šulc, F. Romano, A. A. Louis, J. P. K. Doye, C. Micheletti, L. Rovigatti, TacoxDNA: A user-friendly web server for simulations of complex DNA structures, from single strands to origami. *J. Comput. Chem.* **40**, 2586–2595 (2019).

63. O. Henrich, Y. A. Gutiérrez Fosado, T. Curk, T. E. Ouldridge, Coarse-grained simulation of DNA using LAMMPS : An implementation of the oxDNA model and its applications. *Eur. Phys. J. E* **41**, 57 (2018).

Supplementary Materials

DNA origami fork design, additional TEM and AFM images, correlated Raman-SEM maps, Raman reference spectra, UV-vis absorption spectra, additional SERS spectra, evaluation of the DNA coating layer thickness, plasmonic nanoparticle dimer simulations, calculation of the hot spot volumes, list of DNA strands, caDNAno design of the DNA origami nanofork

Figures

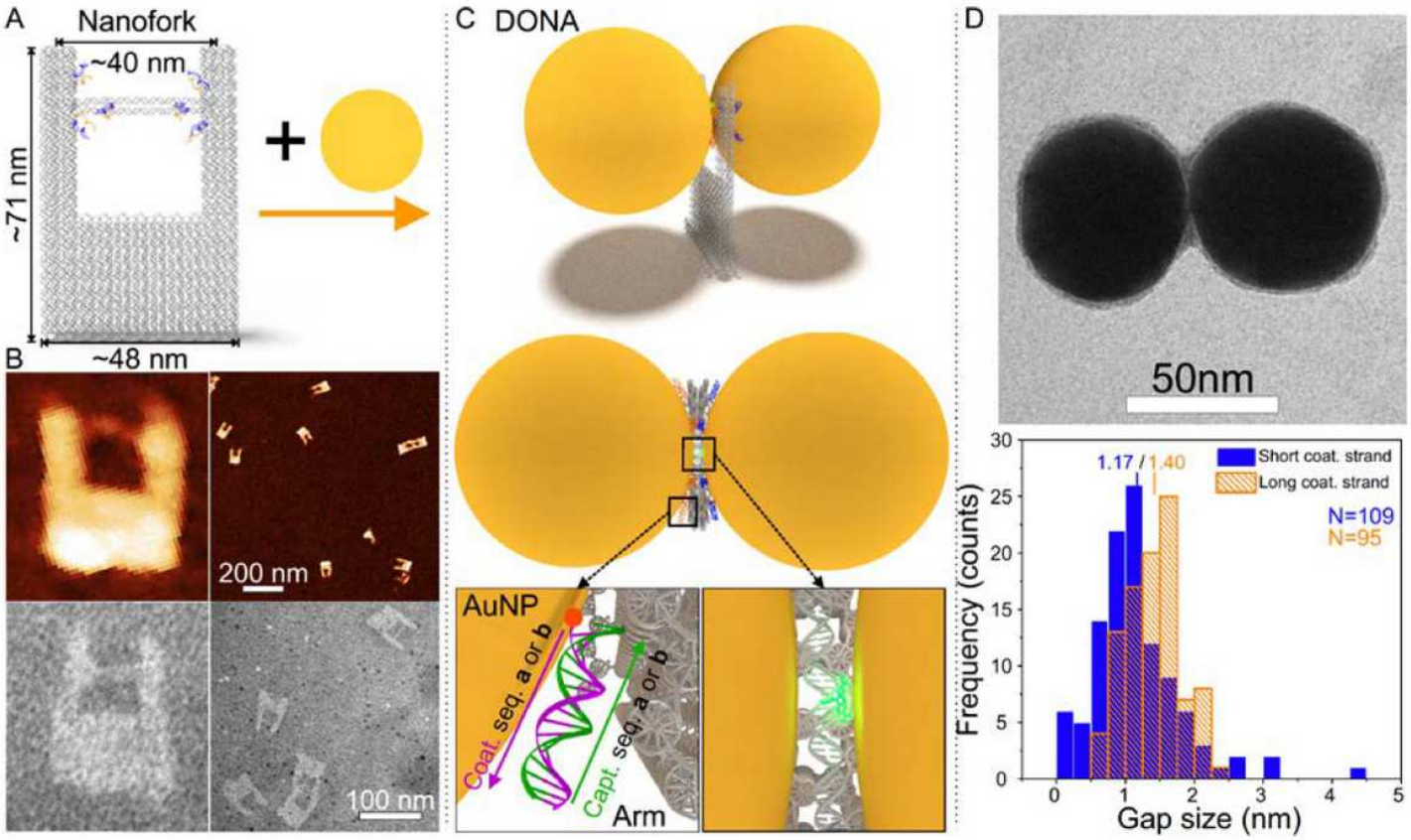

Figure 1

Scheme and characterization of the DONA structures. (A) Schematic representation of the DNA origami nanofork having a DNA bridge that is 90 nt long. (B) AFM and TEM images of the DNA origami nanofork. The sizes of the close-up AFM and TEM images on the lower left are both approx. 90 nm × 100 nm. (C) Two differently coated nanoparticles can be attached selectively via DNA hybridization to the two different sequences of DNA capture strands on the arms and the bridge of the DNA origami to form DONA structures. A side-view and a top-view scheme of the assembled DONA structures is shown. The position of an analyte molecule attached to the DNA bridge is illustrated as a green glow. The DNA hybridisation of nanoparticles and DNA origami in the “zipper” configuration is shown in the insets. (D) Representative TEM image of an assembled smaller gap size Au DONA (more examples shown in Fig. S2), along with distributions of gap sizes determined from TEM images of smaller and larger gap size DONAs with an average gap size of 1.17 and 1.40 nm, respectively. The number of the counted DONAs N was 109 and 95 for the smaller and larger gap size, respectively.

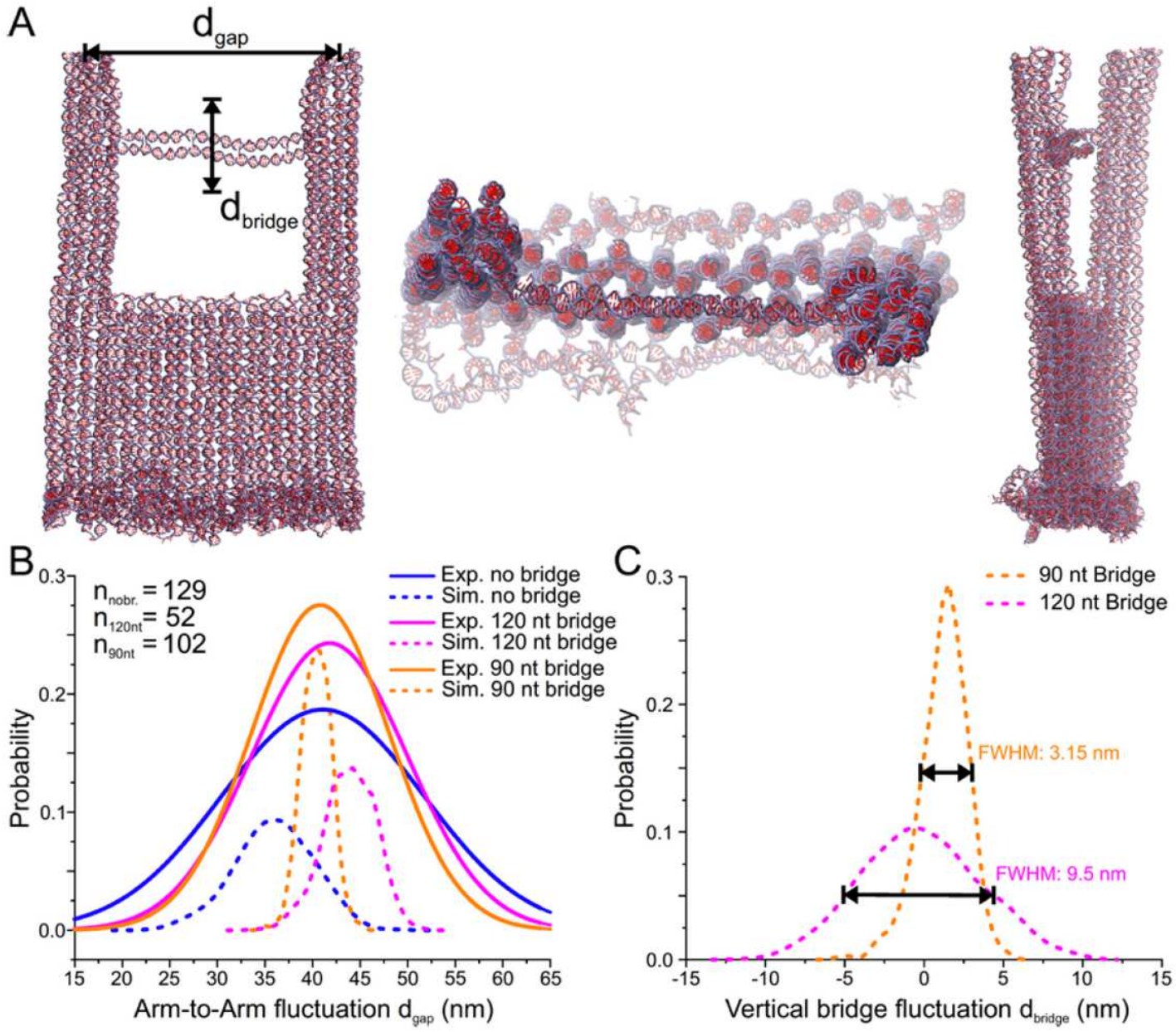

Figure 2

Coarse-grained oxDNA model of the DNA origami nanofork. (A) Snapshots of two side views and one top-view of the nanofork with 90 nt DNA bridge as simulated using the oxDNA model. (B) Plot of the simulated probability distribution of distance between the tips of the two arms and comparison with experimental values obtained from AFM images (for no bridge, 90 nt and 120 nt bridge, the maxima are 41.13 nm, 40.82 nm and 41.84 nm, respectively). The number of nanoforks analysed by AFM is given in the inset. (C) Plot of the simulated probability distribution of the flexibility of the centre of a 90 nt and a 120 nt DNA bridge in respect to the straight bridge position, with the maxima at 1.56 nm and -0.6 nm, respectively.

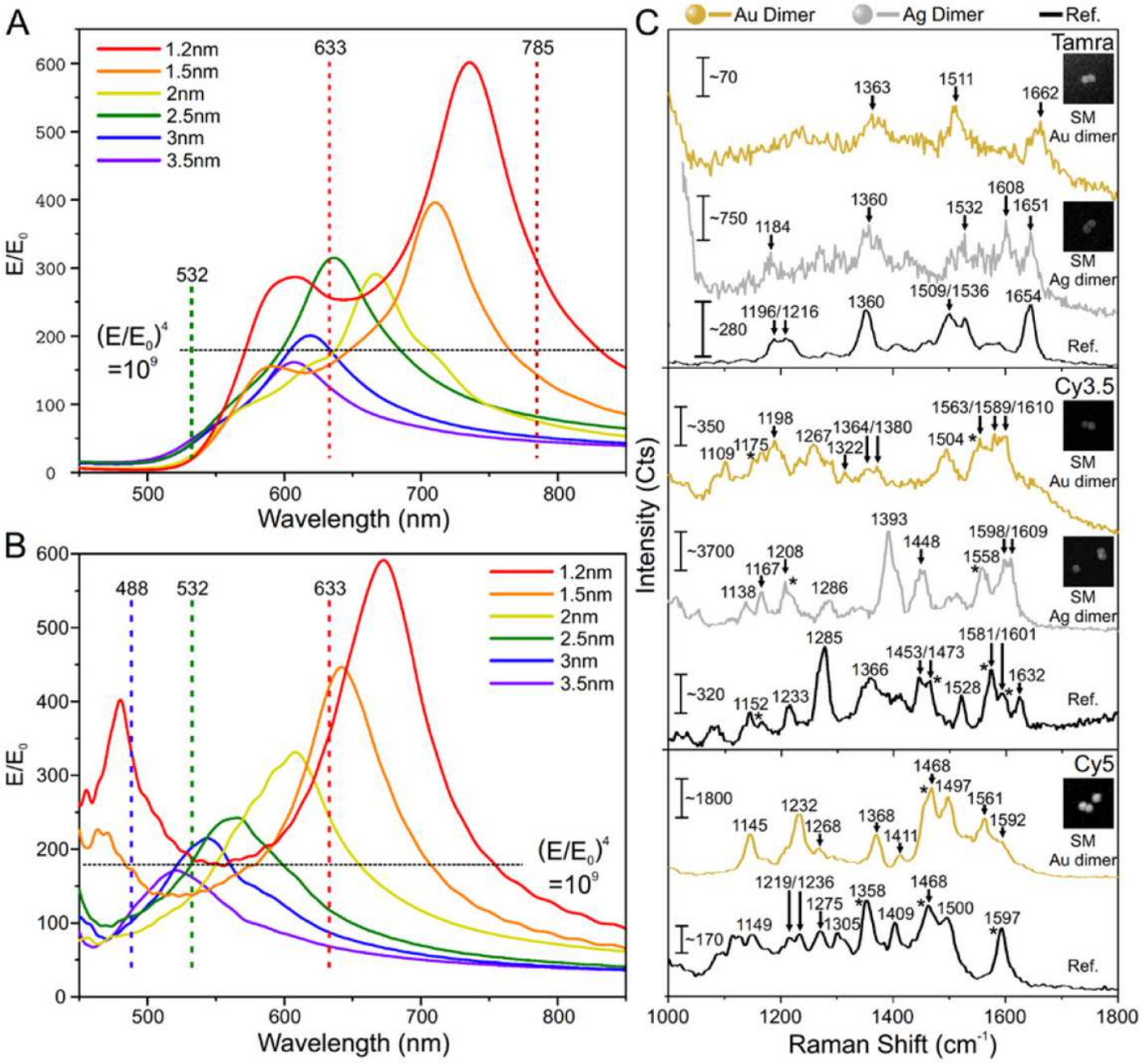

Figure 3

FDTD simulations of DNA coated Au and Ag dimers and single-molecule SERS spectra of different dyes. The dashed line in a. and b. indicates a field enhancement of 109 that is assumed to be the requirement for single molecule detection. (A) FDTD simulations of the E-field enhancement of a Au dimer consisting of DNA coated 60 nm diameter particles on a silicon substrate. (B) FDTD simulations of the E-field enhancement of a DNA coated Ag dimer consisting of 60 nm diameter particles on a silicon substrate. (C) SM SERS spectra of TAMRA, Cy3.5 and Cy5 obtained using Au and Ag DONAs (Cy5 was measured only using Au DONAs). The inset shows SEM images of the specific DONAs, from which the SM SERS spectra have been obtained. The size of the inset SEM images is 450 x 450 nm.

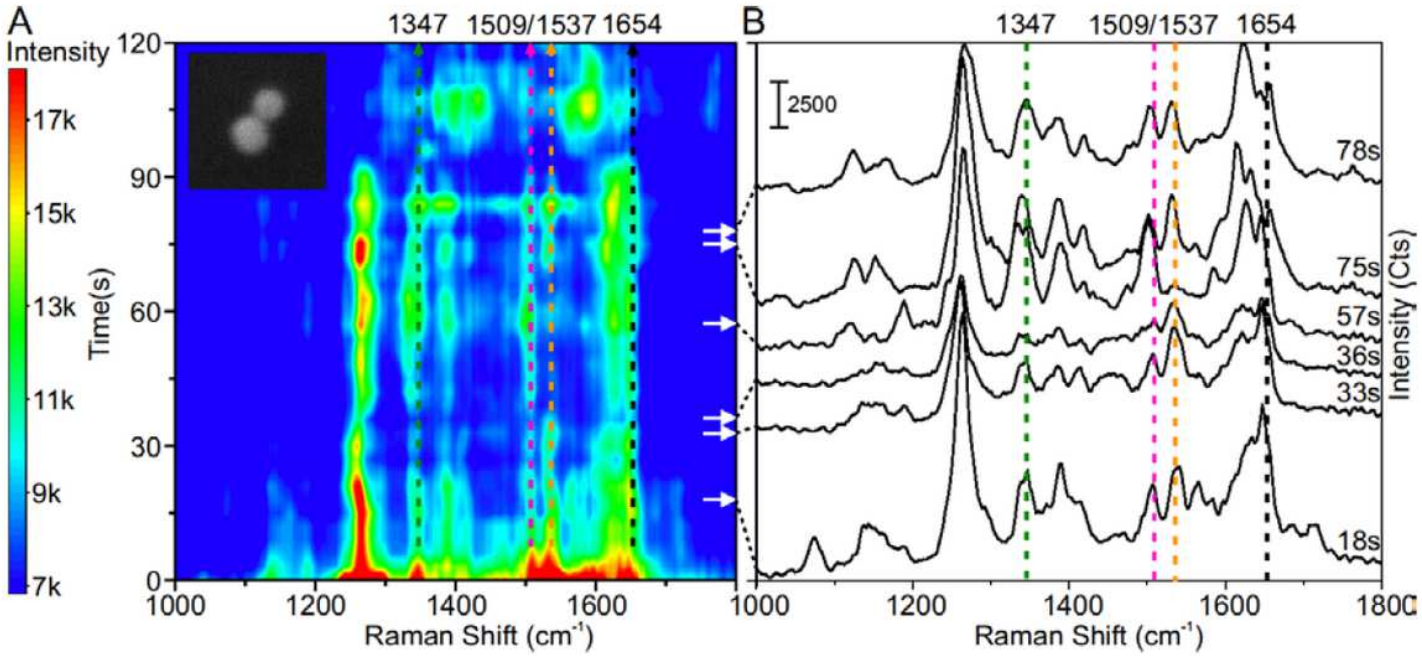

Figure 4

Single-molecule SERS time series measurements of TAMRA. (A) Time vs Raman shift contour plot for a single TAMRA molecule. The dotted lines indicate the main TAMRA peaks (1654, 1537, 1509). The dotted green line indicates a band at 1347, which can be either a shifted TAMRA band or a DNA peak. The white arrows indicate different times at which the SERS spectra shown in B are extracted. The size of the inset image is 500 nm x 500 nm. (B) Full single TAMRA spectra extracted from the contour plot at 48, 63, 66, 87, 105 and 108 s. The same TAMRA bands are indicated with lines as in a.

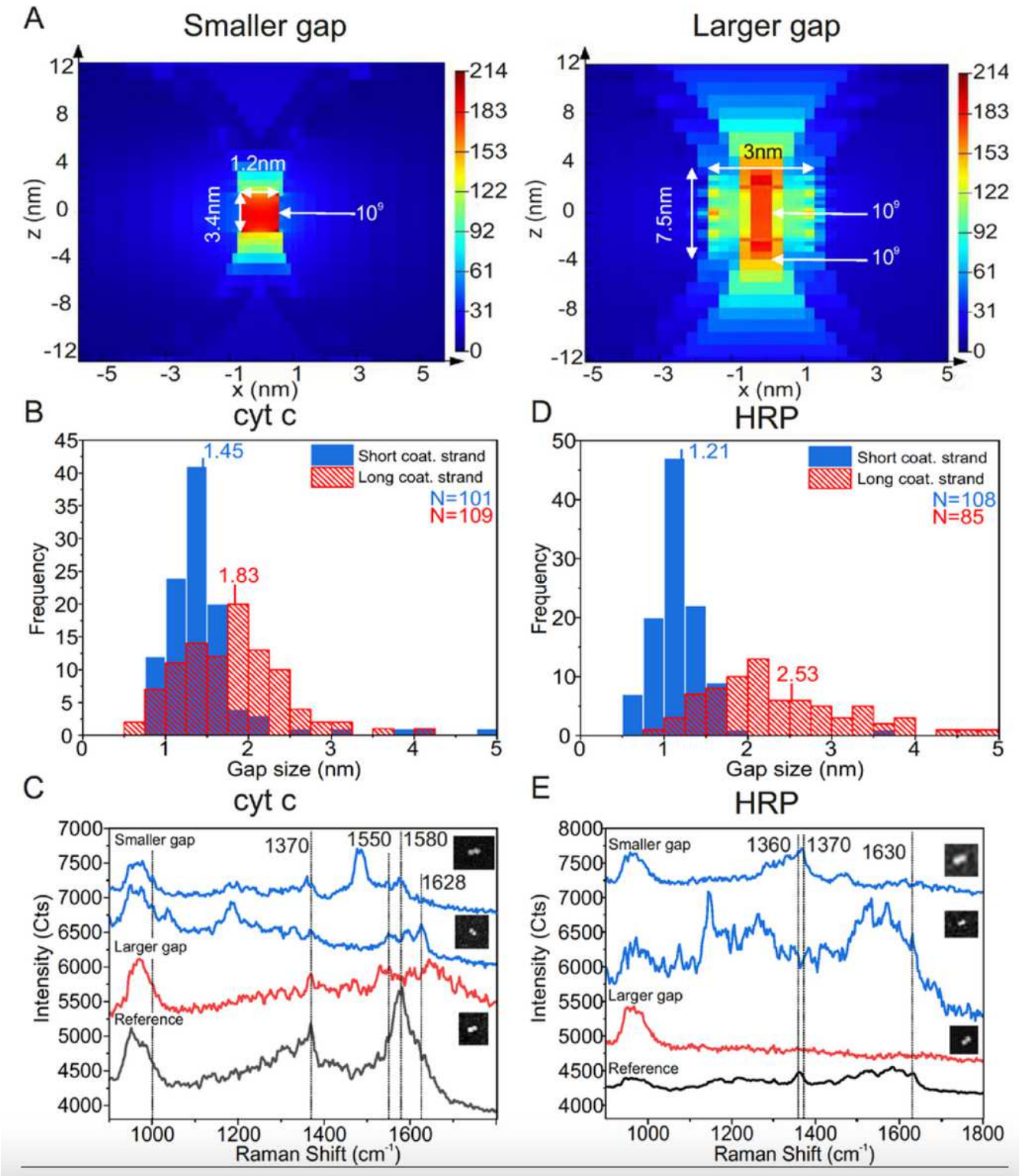

Figure 5

Single-molecule SERS measurements of cytochrome c (cyt c) and horseradish peroxidase (HRP). (A) Field enhancement plots of the DONA Au dimers, when the gap size is 1.2 nm (smaller gap) and 3 nm (larger gap). (B) Distributions of the smaller and larger gap sizes determined from TEM images of cyt c with the average gap sizes of 1.45 nm and 1.83 nm, respectively. The number of counted dimers N was 101 and 109 for the smaller and larger gap, respectively. (C) SM SERS spectra of cyt c using Au DONA structures

and 633 nm excitation. (D) Distributions of the smaller and larger gap sizes determined from TEM images of HRP with the average gap sizes of 1.21 nm and 2.53 nm. The number of counted dimers N was 108 and 95 for the small and large gap, respectively. (E) SM SERS spectra of HRP using Au DONA structures and 633 nm excitation. The insets in C and E show SEM images of the specific DONAs, from which the SM SERS spectra have been obtained. The sizes of the SEM images are from top to bottom 360 × 280 nm, 360 × 420 nm, 300 × 360 nm and 240 × 240 nm 360 x 420 nm 300 x 300 nm, respectively.

Supplementary Files

This is a list of supplementary files associated with this preprint. Click to download.

- 20201222SupportingInformationfinal.pdf